







Mechanochromic Polyurethane Shape Memory Polymer for Biomedical Applications

Thalma Orado¹ | Bethany Yashkus² | Richard Chandardat³ | Samantha Zysk¹ | Zachary J. Geffert¹ | Ernest Emmanuel Obeng¹ | Xiaocun Lu³ | Pranav Soman¹ | Mary Beth B. Monroe¹

¹Biomedical and Chemical Engineering Department, Syracuse University, Syracuse, New York, USA | ²Department of Chemistry and Biochemistry, Wilkes University, Wilkes-Barre, Pennsylvania, USA | ³Department of Chemistry and Biochemistry, Clarkson University, Potsdam, New York, USA

Correspondence: Mary Beth B. Monroe (mbmonroe@syr.edu)

Received: 25 April 2025 | Revised: 17 July 2025 | Accepted: 7 August 2025

Funding: This work was supported by Syracuse University.

Keywords: mechanophore | polyurethane | shape memory polymer | spiropyran

ABSTRACT

The incorporation of functional molecular switches into smart materials imparts dynamic material properties, gaining deeper insight into how molecular structure affects the functionality of these materials and aiding the development of novel sensor devices. To enable mechanochromic biomaterials capable of sensing shape changes, we explored the incorporation of spiropyran (SP) mechanophores into a polyurethane (PUR) shape memory polymer (SMP). SPs reversibly generate variations in fluorescence and visual colors due to conversion from inactivated SP to activated merocyanine (MC) in response to force. We hypothesized that SP-containing PUR (PUR-SP) could undergo simultaneous shape and color changes. Small quantities of SP were dissolved in control PUR solutions with different hard-to-soft segment ratios, and PUR-SP films were formed by solvent-casting. The effect of SP incorporation on material properties, including mechanical, shape memory, thermal, and cytocompatibility, was studied. Mechanochromic behavior was analyzed by straining the films and imaging using a camera and fluorescence microscopy. We also employed a previously developed bacterial protease-responsive PUR SMP to confirm that SP incorporation enables simultaneous shape and color changes in the presence of bacteria. Strained samples showed increased fluorescence (up to 56%, p < 0.05), which was reversed upon shape recovery. Mechanochromic behavior was affected by the hard-to-soft segment ratio of the PUR, SP concentration, and strain percentage. Bacteria-responsive PURs with SP showed reduction in fluorescence and complete biofilm removal after incubation with Staphylococcus aureus for 24h, which conveyed the potential to use SP in PURs as a molecular force probe with color-based bacteria detection. This technology could be expanded to include a range of other stimuli-responsive functionalities in future work to enable shape and color changes based on environmental cues.

1 | Introduction

Over the past few decades, smart materials have gained the interest of numerous researchers due to the nature of diverse potential applications in various fields, including medicine [1, 2]. More precisely, stimuli-responsive smart materials have a wide variety of applications as biomaterials. These materials have internal "switches" that can be turned "on" or "off"

reversibly upon application of external stimuli, giving a greater advantage in applications over their static counterparts [3–5]. However, knowledge gaps exist in understanding the mechanisms of transmission of force or signal from one interface to another (i.e., from the biomaterial to the tissue and vice versa) both at the macro and micro level [6–8]. Additionally, robust methods to measure, accurately model, and predict these signals across spatial and temporal scales have yet to

This is an open access article under the terms of the Creative Commons Attribution License, which permits use, distribution and reproduction in any medium, provided the original work is properly cited.

© 2025 The Author(s). Journal of Biomedical Materials Research Part A published by Wiley Periodicals LLC.

be established [9–13]. Incorporation of functional molecular switches, particularly those with multiple hydrogen-bonding groups, into smart materials can impart dynamic material properties and gain fundamental insight into how molecular structures affect materials' functionality [14, 15]. In addition, they facilitate the development of smart materials for novel sensors and actuator devices.

Previously, we synthesized a segmented thermoplastic polyurethane (PUR) for potential biomaterials [1, 16]. To further enhance its capability as a sensor material, we sought to incorporate mechanophores, which are mechanically sensitive molecular switches, to develop a mechanochromic PUR [17-19]. Mechanochromic polymers are smart materials that reversibly generate variations in fluorescence and optical colors in response to mechanical force, providing visible color-based presentation of the stress-relaxed state of polymers [20, 21]. This property makes them suitable for applications such as stress sensing, information processing, and damage detection [20, 22, 23]. Current approaches to generating mechanochromic polymers involve the incorporation of mechanophores into polymer matrices, with a focus on enhancing stress transfer efficiency from the polymer to the mechanochromic compound [22, 24]. Spiropyrans (SPs) are classical mechanophores well studied in literature and shown to respond to both ultraviolet light and mechanical force in many different polymeric materials [25-27]. Their color changes in response to mechanical force due to the conversion from the ring-closed SP structure to its corresponding ring-open merocyanine (MC) structure. This change is reversible, and the original SP color is recovered after removal of the mechanical force [22, 28, 29].

Due to their excellent mechanical properties, adjustable chemical structure, and low glass transition temperatures, segmented thermoplastic PUR matrices have been shown to be effective for fabricating mechanochromic polymer composites [21, 29–31]. Segmented thermoplastic PUR shape memory polymers (SMPs) are ideal for making mechanochromic polymers because they can be deformed and maintained in a secondary shape after a specific thermal treatment due to a balance between soft and hard segments. After applying another thermal treatment, the SMPs revert to the original shape [1, 30–33]. Polymers with both mechanochromic and shape memory properties will therefore achieve a temporary color and shape change during the initial programming, which are both reversible. Mechanochromic SMPs provide opportunities for the innovative design of optically responsive and multifunctional sensor biomaterials for biomedical use. For instance, orthotic devices for at-home use with mechanochromic components could measure and monitor the stress and strain exerted by the human body [34, 35]. Additionally, mechanically responsive biomaterials can induce mechanical perturbations in vitro that transduce optical signals that could be captured by functionalized biological reagents for medical significance. Finally, these materials could serve as wound infection sensors by adding a bacteria-responsive component to the polymer backbone, which would enable shape and color changes in the presence of bacteria to alert clinicians and patients to wound infections.

Some researchers have achieved mechanochromic SMPs by incorporating mechanophores into the polymers. These

mechanochromic polymers exhibit color change when stress is applied, which can be recovered upon heating or application of a secondary stimulus such as visible light or heat [36-39]. To achieve mechanochromic responses, SPs can be covalently linked to the backbones and crosslinkers of polymer matrices [20, 25, 26, 40, 41]. In addition, intermolecular interactions, such as hydrogen bonding between the SP and polymer, play an important role in the development of mechanochromic behavior when force is applied to the material [23, 26, 41]. Since color response in mechanochromic polymers results from transducing external stress to the SP through the polymer matrix, effective bonding between the polymer and SP is essential to achieve an efficient stress loading from the polymer to SP. [17, 42, 43] Our library of segmented thermoplastic PURs is easy to synthesize and has high tunability in terms of chemical, mechanical, and shape memory properties. These PURs hold great potential as smart sensing biomaterials, especially with the incorporation of diverse molecular switches that allow for tailored shape recovery cues (e.g., magnetic, enzymatic, light, etc.) [1, 16, 44].

In this work, we were able to achieve a predictable stress activation of SP within mechanochromic PURs, which could be recovered upon heating to regain their original shape. SPs have been physically crosslinked at different concentrations into segmented thermoplastic PURs with varying hard-to-soft segment ratios. The influence of SP concentration, SP incorporation mechanism, polymer matrix rigidity, and polymer straining, as well as the influence of shape memory properties on mechanochromism is presented here.

Additionally, as a proof of concept, we incorporated SP into a previously developed bacterial protease-responsive PUR SMP [38]. After programming this SMP into a secondary shape, it exhibits shape recovery in the presence of bacterial proteases. The shape change provides a visual cue for bacterial presence while simultaneously inhibiting biofilm formation. Here, we developed SP-containing bacterial protease-responsive SMPs as a prototype mechanochromism SMP biomaterial. Their shape deformation, color change, and biofilm formation were measured during a biofilm assay with *Staphylococcus aureus*. This work demonstrates the strong potential of this technology for application in environmental sensing.

2 | Experimental Section

2.1 | Materials

Hexamethylene diisocyanate (HDI, Thermo Fisher Scientific, Waltham, MA), triethylene glycol (TEG, Fisher), polypropylene glycol (PPG, MW 2000 g mol⁻¹, Fisher), tetrahydrofuran (THF, Fisher), dibutyltin dilaurate (DBTDL) catalyst (Sigma), diethyl ether anhydrous (Fisher), NaOH (Sigma-Aldrich, Burlington, MA), phosphate buffered saline (PBS, Fisher), Dulbecco's Modified Eagle's Medium (DMEM, Fisher), penicillin–streptomycin (P/S, Fisher), fetal bovine serum (FBS, Fisher), ethanol (reagent alcohol, Fisher), sodium hydroxide (Fisher), polyglutamic acid (PGlu, Thermo Fisher Scientific, Waltham, MA [Fisher]), lysogeny broth (LB, Sigma), *S. aureus*, and A375 fibroblasts (ATCC, Manassas, VA, USA) were purchased as indicated above and used as received unless otherwise specified.

2.2 | SP Synthesis

The synthesis of hydroxy-SP was optimized based on a previously reported procedure [45]. 2-hydroxyethyl-2,3,3-trimethyl-3 H-indolium iodide (5.17g, 15.6 mmol, 1.0 equiv) and 2,3-dihydro xy-5-nitrobenzaldehyde (2.86g, 15.6 mmol, 1.0 equiv) were dissolved in 100 mL absolute ethanol, followed by the addition of piperidine (4.37 mL, 31.2 mmol, 2 equiv). The reaction mixture was refluxed at 100°C for 12h and concentrated in vacuo. After vacuum filtration, the precipitates were collected and washed with cold ethanol to yield black powder without further purification. (3.96 g, 10.7 mmol, 69%).

2.3 | Segmented Thermoplastic PUR Synthesis

The segmented thermoplastic PUR used in this study was synthesized according to a previously described method [16]. Briefly, PURs with varying hard segments (Table 1) were synthesized using a one-step solvent-free process. Twenty-four hours prior to synthesis, the soft segment, PPG, and the chain extender, TEG, were dried in a 50°C controlled vacuum oven. HDI, used as the hard segment, was combined with PPG and TEG and placed in a speed mixer cup in a moisture-controlled glove box (Labconco, Kansas City, MO, USA). DBTDL was added as a catalyst. The cup was then placed in a Speed Mixer (Flacktek, Landrum, SC, USA) and mixed at 3500 rpm for 30 s. This mixture was poured into a Teflon liner and allowed to cure at 50°C for 48 h.

Fourier transform infrared spectroscopy (FTIR) (Nicolet iS5, Fisher Scientific, Waltham, MA, USA) was used to ensure successful synthesis by the formation of characteristic urethane peaks at $\sim\!3320\,\mathrm{cm^{-1}}$ (N–H stretching) and $\sim\!1677\,\mathrm{cm^{-1}}$ (NHCOO stretching), and no peak at $\sim\!2270\,\mathrm{cm^{-1}}$, indicating complete reaction of NCO.

2.4 | Physical Crosslinking of SP Into PUR

To make PUR/SP films, 2g of premade PUR were dissolved in 20 mL chloroform for ~1 h. Small amounts of SP (0.31, 0.63, 1.25 and 2.5 mg) were dissolved in the PUR solution. The resultant solutions were poured into Teflon molds, and the solvent was evaporated, leaving behind 15 distinct PUR-SP films, as

Sample ID	Formulation	HDI (mol %)	PPG (mol %)	TEG (mol %)
4HDI	4.2 HDI: 1 PPG: 3.2 TEG	50	12	38
5HDI	5.2 HDI: 1 PPG: 4.2 TEG	50	10	40
6HDI	6.2 HDI: 1 PPG: 5.2 TEG	50	8	42

described in Table 2. These films were stored in the dark for later use in characterizing photochromic behavior. The PUR/SP film was exposed to white light for 1 h to ensure complete conversion of any residual MC to the SP form prior to use.

2.5 | Preparation of Bacteria Protease-Responsive PUR With SP (5HDI-PEP-SP)

A 100 mL round-bottomed flask was charged with HDI (2.2g, 0.0131 mol), PPG (6.25 g, 0.046 mol), and DBTDL catalyst (15 µL). The flask was placed in an oil bath, and the temperature was increased to 80°C gradually over a period of ~2h (to prevent HDI gelation), and the mixture was stirred while purging with nitrogen. After 24 h, TEG (1.97 g, 0.0132 mol) was dissolved in dry THF (5mL) and added to the flask while stirring. After ~1.5-3h, additional HDI (1.6g, 0.09 mol) and Boc-protected PGlu (10 mg, 3.33×10^{-6} mol) in 10 mL DMSO were added to the flask and allowed to stir for 18 h. Successful PUR-PEP synthesis was confirmed by FTIR as indicated by the introduction of the C=O amide peak at ~1600 cm⁻¹ in addition to the urethane NH and CO peaks at ~3320 and 1677 cm⁻¹, respectively. Finally, SP (2.5 mg, 0.007 mmol) dissolved in 1 mL THF was added to the flask via stirring while purging with nitrogen for 30 min, resulting in SP-containing 5HDI-PEP. Afterward, the viscous reaction solution was poured into Teflon dishes and left at ambient temperature for the solvent to evaporate before transferring to a vacuum oven at 50°C for 2h to dry. The resultant films were peeled from the Teflon dish and kept in the dark prior to characterization.

2.6 | Thermal, Mechanical and Shape Memory Properties

2.6.1 | Thermal Analysis

Differential scanning calorimetry (DSC) was carried out using a Q2000 instrument. Samples (n=3, $3-5\,\mathrm{mg}$) were equilibrated for 2 min, heated to $110^\circ\mathrm{C}$ at $10^\circ\mathrm{C}\,\mathrm{min}^{-1}$, kept isothermally for 2 min, cooled to $50^\circ\mathrm{C}$ at $5^\circ\mathrm{C}\,\mathrm{min}^{-1}$, kept isothermally for 2 min, cooled to $-10^\circ\mathrm{C}$, kept isothermally for 2 min, and finally reheated to $120^\circ\mathrm{C}$ at a rate of $10^\circ\mathrm{C}\,\mathrm{min}^{-1}$. Glass transition (T_g) and melting (T_m) temperatures were determined from the second heating cycle measurements as the midpoint of the inflection on the thermogram and the minimum value of the endothermic melting peak, respectively.

TABLE 2 | PUR-SP film formulations—expressed as w/w percent.

4HDI	5 HDI	6HDI	
4 HDI-0% SP	5 HDI-0% SP	6 HDI-0% SP	
4 HDI-0.015% SP	5 HDI-0.015% SP	6 HDI-0.015% SP	
4 HDI-0.032% SP	5 HDI-0.032% SP	6 HDI-0.032% SP	
4 HDI-0.063% SP	5 HDI-0.063% SP	6 HDI-0.063% SP	
4 HDI-0.126% SP	5 HDI-0.126% SP	6 HDI-0.126% SP	

2.6.2 | Mechanical Analysis

Dog bone-shaped samples were punched from the PUR-SP films (n=3) and then loaded onto an Instron 3344 Universal Test Instrument (Norwood, MA, USA) with a 24N load cell. Samples were strained at a rate of $10 \, \mathrm{mm \, min^{-1}}$ until fracture to determine the films' Young's modulus, tensile strength, and elongation at break from resulting stress/strain curves.

2.6.3 | Shape Memory Properties

Dog bone samples (n=3) were punched from the PUR-SP films and loaded onto a TA Instruments Q800 in controlled-force mode. In three cycles, the samples were heated to $60^{\circ}\mathrm{C}$ at a heating rate of $2^{\circ}\mathrm{C\,min^{-1}}$, strained 40% at $0.03\,\mathrm{N\,min^{-1}}$, and then cooled to $-5^{\circ}\mathrm{C}$ at a rate of $2^{\circ}\mathrm{C\,min^{-1}}$ to ensure complete fixation of the temporary shape. Samples were then unloaded at $0.1\,\mathrm{min^{-1}}$ and reheated to $60^{\circ}\mathrm{C}$ at a rate of $2^{\circ}\mathrm{C\,min^{-1}}$ to measure the recovery ratio (R_{r}) . Recovery (R_{r}) and fixing (R_{f}) ratios were calculated using the equations below, where ε_{u} is the strain after unloading (fixed shape), N is the cycle number used for the study, which is 2 in our case, $\varepsilon_{\mathrm{m}}(L)$ is the maximum strain at loading, and ε_{p} is the remaining strain after recovery (permanent strain).

$$R_{\rm f}(X) = \frac{\varepsilon_{\rm u}}{\varepsilon_{\rm m}(L)} \tag{1}$$

$$R_{\rm r}\left(N\right) = \frac{\varepsilon_{\rm m} - \varepsilon_{\rm p}(N)}{\varepsilon_{\rm m} - \varepsilon_{\rm p}(N-1)} \tag{2}$$

2.7 | Cytocompatibility Assay

To ensure cell viability would not be affected by the catalyst used to synthesize the PUR, 5g of control PUR was dissolved in ~200 mL chloroform and then precipitated using ice-cold diethyl ether (500 mL), filtered, and allowed to dry in a hood. The dry polymer was washed in deionized water by sonicating for 7 days and changing the water daily. PUR-SP films were made as previously outlined.

Cytocompatibility was tested on a control PUR and PUR with 0.126% (w/w) SP (maximum SP concentration) using A375 cells (passage 7). Samples were cut into small circles using a 6 mm biopsy punch and washed with deionized water and PBS. These samples were then sterilized using UV light. Cells were maintained in DMEM supplemented with 10% FBS and 1% PS at 37°C for 72h. Cells were seeded at 10,000 cells per well in a 24-well plate for 24h at 37°C/5% CO₂. Then, sterilized samples were placed in Transwell inserts above the seeded cells. Wells with empty inserts containing 10% ethanol in media and empty inserts with media only were utilized as negative (cytotoxic) and positive (cytocompatible) controls, respectively. After 24h, the Transwells were removed, and a live/dead assay (Thermo Fisher Scientific) was used to evaluate cytocompatibility. Live (Calcein AM, green) and dead (BOBO-3 iodide, red) stains were applied to the cells for ~20 min. The media was removed, and the cells were washed with PBS three times. Cells were visualized using fluorescence microscopy, and percent viability was then calculated as in the equation below and later normalized to the original seeding density.

$$\%$$
 cell viability = $\frac{\text{live cells}}{\text{live cells} + \text{dead cells}} \times 100\%$

2.8 | Analysis of Mechanochromic Behavior

2.8.1 | Activation of SP by Manual Stretching and Heat-Based Recovery

Prior to characterization, dog bone (ASTM D638 type IV) samples (n=5) with a gage length of 6.25 mm and a width of 1.5 mm were cut from the prepared films. These samples were left in ambient light for 24 h and exposed to an LED light for 1h to facilitate a full conversion of residual MC into SP. Images of these samples were taken pre- and post-light exposure to assess any visual color change. One sample was kept unstrained, and the remaining four were heated at 95°C for 5–7 min in an isothermal oven, strained to roughly 30%, 60%, 80%, and 100% using an Arduino controlled custom-made straining device (Figure S1), and allowed to cool to room temperature before removing from the straining device. Samples were imaged with a camera before and after straining to monitor any visual color changes. Samples were then imaged using the green channel under fluorescent microscopy. ImageJ was used to quantify the total fluorescence of each image (n=3)per sample).

To assess the effect of shape recovery on mechanochromism, strained samples were placed in an oven at 95°C for 5 min to return the polymer to its original shape. Images were taken before and after this process to assess any visual color reversal. Fluorescence microscopy was then used as described above to analyze changes in fluorescence.

2.8.2 | Activation of SP Under Tensile Testing

Dog bone-shaped samples were punched from the 5HDI-SP films and investigated under a strain rate of $10\,\mathrm{mm\,min^{-1}}$ using an Instron 3344 Universal Test Instrument (Norwood, MA, USA). The samples were unloaded from the machine at different phases of mechanical deformation and at fracture, and representative fluorescent images were taken. To determine the precise value of the minimum strain that activates the SP, fluorescence intensity image analysis was performed on the images using Image J software.

2.8.3 | Ultraviolet-Visible Light Spectrophotometry

The mechanochromic response resulting from the difference in concentration of SP in the PUR was measured as a function of absorbance using an ultraviolet–visible light (UV–vis) spectrophotometer (Evolution 201/220 UV–Visible Spectrophotometers Thermo Scientific). Samples were cut $(15\times8\times0.037$ [thickness] mm) from the 5HDI-SP films with various concentrations of SP using a rectangular die. These samples were strained to 130%–150% strain using the straining device to activate the SP in the

polymer matrix. Immediately, the samples were transferred into the UV Vis spectrophotometer using a sample holder specifically designed for this purpose. The samples were scanned from 300 to 600 nm at room temperature. Unstrained samples were analyzed as controls.

2.8.4 | Dynamic Analysis of Mechanochromism

A 5HDI-0.063% SP dog bone sample was loaded onto a TA Instrument Q800 dynamic mechanical analyzer in controlled-force mode. The sample was heated to 60°C at a heating rate of 2°C min⁻¹, strained to 40% strain at 0.03 N min⁻¹ and cooled to -5°C at a rate of 2°C min⁻¹ to ensure complete fixation of the temporary shape. Samples were then unloaded at 0.1 N min⁻¹ and reheated to 60°C at a rate of 2°C min⁻¹ to allow for recovery. In between the heating, straining, cooling, unloading, and recovery steps, the furnace was opened, and images of the sample were captured while shining a UV lamp on it.

Changes in fluorescence in the 5HDI-SP samples during recovery were further assessed by confocal microscopy. 5HDI-0.063% SP samples strained to 150% using the straining device (S1) were placed in water (to reduce their $T_{\rm g}$ as previously described) [1]. The samples were mounted onto a Zeiss LSM 980 Confocal Laser scanning microscope stage heated to 45°C to allow for recovery. Split-channel 3D imaging was carried out, with one channel (405–525 nm) capturing the inactivated (SP) emission, while the second channel (540–725 nm) was chosen to collect the activated (MC) probe emission. Strained and unstrained samples were imaged without the heated stage to study changes in fluorescence.

2.9 | Biofilm Removal Assay

Samples were cut $\sim 15 \times 5 \times 0.04$ (thickness) mm from the following sample films: control PUR (5HDI), control PUR with SP (5HDI-SP), bacterial protease-responsive PUR (5HDI-PEP), and SP-functionalized bacterial protease-responsive PUR (5HDI-PEP-SP). These samples were strained to 130%-150% strain using the straining device and imaged using fluorescence microscopy. A biofilm assay was conducted according to a previously outlined protocol [44]. Briefly, after sterilizing the films with UV light, they were placed in 24-well plates. LB was added to the wells together with S. aureus grown to O.D. 0.4, and the plates were incubated for 24h. Samples were washed with 0.85% NaCl solution, fixed with 2.5% glutaraldehyde for 1h, and dried with increasing concentrations of ethanol. Dried samples were imaged using scanning electron microscopy (SEM) (Jeol JSM 5600, Tokyo, Japan) at 1500-2000× magnification and 15-20 kV high vacuum. Additionally, samples were imaged using fluorescence microscopy, and their final dimensions were measured using calipers to determine R_r .

2.10 | In Vitro Release of SP From PUR-SP Films

The release of SP was investigated under physiological conditions. For this study, 5HDI-0.063% SP and 5HDI-PEP-SP films of

 15×5 mm dimensions were cut from PUR-SP films and weighed to determine loaded SP content. These samples were immersed in 5 mL of PBS and incubated at 37°C under shaking for 192 h while maintaining dark conditions. At pre-determined time intervals, 1 mL of the medium was taken as the release sample and replaced with fresh PBS. The concentrations of SP in the release samples were measured by a micro-plate reader (Biotek Synergy microplate reader, BioTek Instruments) at 540 nm.

2.11 | Statistical Analysis

All data is expressed as the mean±standard deviation from triplicates for each experiment. Unpaired *T*-tests were used to compare two groups while one-way ANOVA followed by Tukey–Kramer post hoc correction was used to compare more than two sample groups. A *p*-value of less than 0.05 was considered statistically significant. All data were managed using Microsoft Excel Software, and statistical analyses were done using GraphPad Prism version 10.4.1 for Windows.

3 | Results and Discussion

3.1 | Effect of SP Incorporation on Polymer Properties

3.1.1 | Mechanical Properties

Representative stress–strain curves of PUR-SP samples are shown in Figure S2. Tensile testing data indicate that the addition of small quantities of SP significantly improved the mechanical properties of the PURs (Figure 1). For instance, the tensile modulus and tensile strength of the 5HDI-SP samples improved ($F_{(4,10)}=[16.94],\ p=0.0002$ and $F_{(4,10)}=[7.250],\ p=0.0052$ respectively) with increased SP concentration. Although the elongation at break also improved with increased SP concentration, the difference was not significant ($F_{(4,10)}=[2.190],\ p=0.1435$). Physically crosslinking SP into our PUR enabled us to achieve elastic films with high strength, which is relevant to our targeted biomedical applications.

These improvements in mechanical properties were anticipated due to hydrogen bonding between the urethane groups of the PUR polymers and the hydroxy groups of SP, enabling the use of SP as a physical crosslinker for the system [22, 46, 47]. Other studies have found similar trends, where the addition of small quantities of SP into a polymer matrix leads to an increase in mechanical properties. In these prior studies, the mechanical properties decline when more SP (> 1.5%) is added [22]. Additionally, when the hard-to-soft segment ratio increased (e.g., from 4HDI to 6HDI), the mechanical strength also increased due to the resulting adjustment in the microphase structure, as previously shown [16]. Thus, mechanical properties can be tuned with both varied hard segment ratios and SP concentrations.

3.1.2 | Thermal Properties

According to the DSC thermograms (Figure S4), the $T_{\rm g}$'s of PUR samples range from 65°C to 70°C, while $T_{\rm g}$'s of the PUR-SP

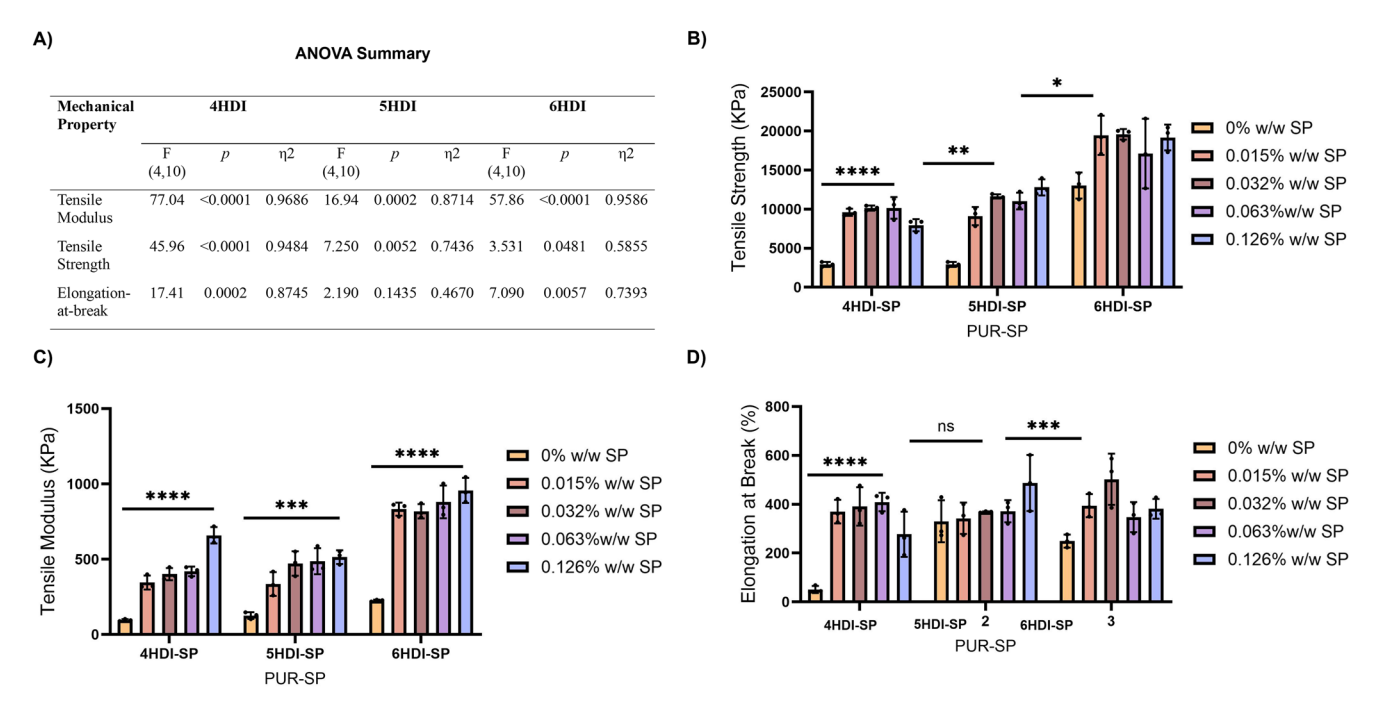


FIGURE 1 | Mechanical properties of SP-containing PURs. (A) One-way analysis of variance summary, (B) tensile strength, (C) tensile modulus, and (D) elongation-at-break. Mean \pm standard deviation displayed, n = 3, **** $p \le 0.0001$, *** $p \le 0.001$, *** $p \le 0.01$, and * $p \le 0.05$ relative to control (sample without SP); ns, not significant.

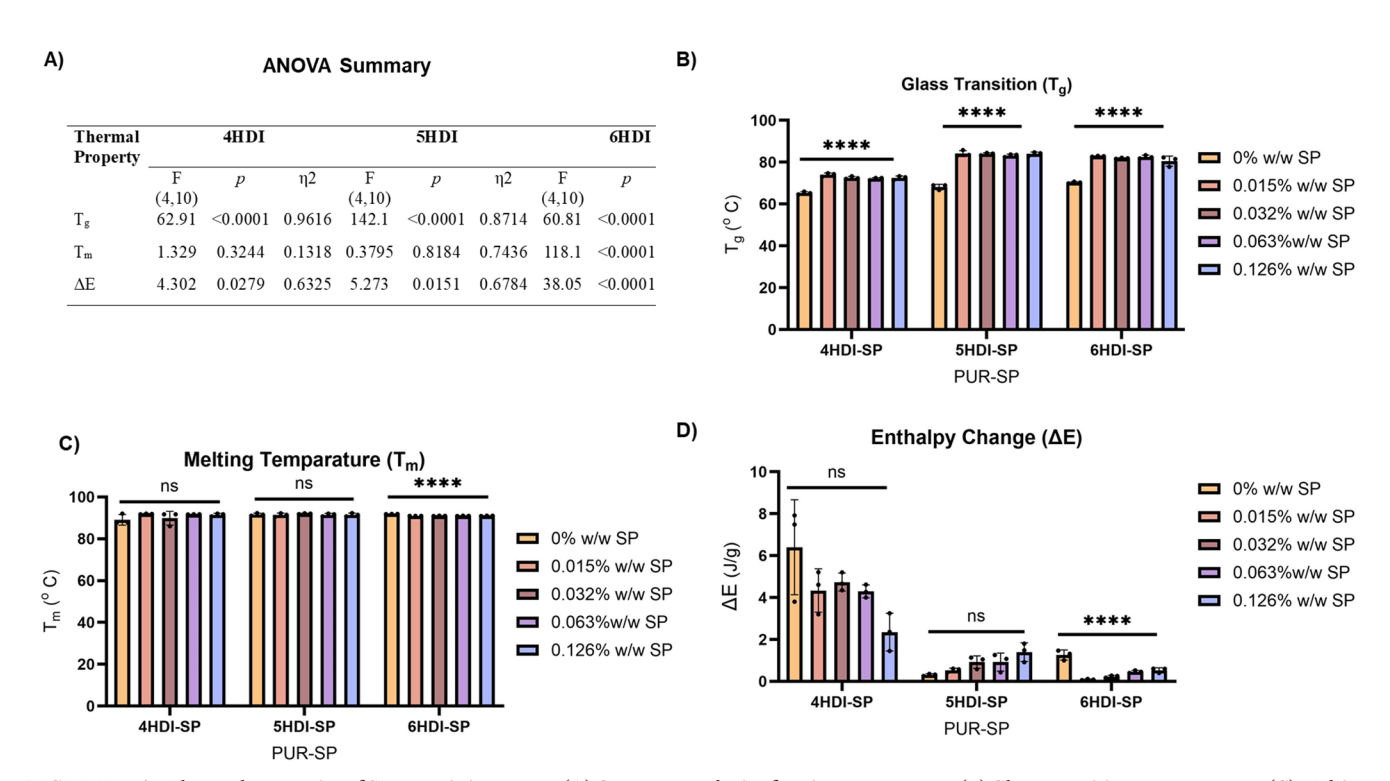


FIGURE 2 | Thermal properties of SP-containing PURs. (A) One-way analysis of variance summary, (B) Glass transition temperatures, (C) Melting temperatures, and (D) Changes in enthalpy. Mean \pm standard deviation displayed, n = 3, **** $p \le 0.0001$ relative to control (sample without SP).

samples range from 72°C to 84°C (Figure 2b). Melting points $(T_{\rm m})$ range from 89°C to 91°C and 89°C to 93°C for the PUR samples and PUR-SP samples, respectively (Figure 2c). Figure 2a shows a summary of ANOVA whereby the addition of the SP caused an increase in $T_{\rm g}$ of all samples ($p \le 0.0001$). Only the $T_{\rm m}$ of 6HDI-SP samples increased significantly ($p \le 0.0001$), while that of 4HDI-SP and 5HDI-SP remained consistent (p = 0.32

and p = 0.81 respectively). The ΔE of 4HDI-SP and 6HDI-SP decreased significantly (p = 0.03 and $p \le 0.0001$ respectively) while that of 5HDI-SP increased (p = 0.02).

The observed increase in $T_{\rm g}$ with SP incorporation can be attributed to the hydrogen bonding between the SP crosslinker and the PUR polymer chains. Since SP has rigid spiro cyclic

structures, it was expected that as the SP physical crosslinker content increased, the PUR matrix would be more rigid, causing the T_{σ} to rise. The rise in ΔE in 5HDI-SP can also be attributed to increased secondary molecular interactions [41, 48]. As the SP content increased, there were more interaction sites for hydrogen bonds between SP and polymer chains. The decrease in ΔE in 4HDI-SP and 6HDI-SP indicates that the SP crosslinkers may disrupt crystal formation in PURs with lower and higher hard segment contents. Thus, there is an optimum amount of hard segment content in the segmented PURs for which SP acts as a crosslinker that stiffens chains and increases crystallinity. SP addition causes a notable decrease in enthalpy, likely due to disruption of hydrogen bonding within the PUR as SP molecules interfere with the strong urethane-urethane interactions in the hard segments and disturb the microphase-separated structure of segmented PUs, which has been previously observed in polyether PURs [49]. This disruption reduces the energy required for thermal transitions. However, with further increases in SP concentration, a slight recovery in enthalpy is noted. This change may be due to the emergence of SP-SP interactions, which serve as physical crosslinking sites between polymer chains to partially restore the thermal energy required to disrupt the system [49].

In addition, the drop in ΔE in 5HDI and 6HDI samples may be a result of increased hard segment content, which also disrupts the microphase structure of the PUR. When hardsegment content increases in polyether PURs, the hard segment domains interfere with the formation and mobility of soft segment crystals. While the crystallinity of the soft segment decreases, hard segments themselves become more crystalline. Moreover, increasing chain extender content causes distinct hard segment melting in DSC. Thus, with increased hard segment content, the total ΔH_m drops sharply because high-enthalpy soft transitions are replaced with low-enthalpy hard transitions [50]. All transition temperatures are above body temperature; when PUR-SP films are used as biomaterials, they will be stable and will recover their primary shape only when subjected to a controlled stimulus and/or increased temperature above body temperature, preventing passive actuation of the SMP material after application.

3.1.3 | Shape Memory Properties

Dynamic mechanical analysis (DMA) data (Table 3) reveals that despite the addition of the SP into the PUR, the shape $R_{\rm f}$ and shape $R_{\rm r}$ were relatively consistent. While the pure PUR samples had $R_{\rm f}$ that ranged between 0.77 and 0.83, PUR-SP samples had fixing ratios between 0.73 and 0.85. On the other hand, $R_{\rm r}$ ranged from 0.94 to 0.96 and from 0.90 to 0.96 for PUR and PUR-SP samples, respectively. Overall, the incorporation of SP did not negatively impact shape memory properties based on the measured $R_{\rm f}$ and $R_{\rm r}$. The shape memory effect is driven by the thermal properties of the soft and hard segments of the PUR polymer matrix. The material is able to fix a temporary shape after heating and straining and return to its original shape upon heating [51]. In addition, this free movement of the chains back to their original shape allows isomerization of the SP molecules.

When the material is heated to a temperature above the $T_{\rm g}$ of the hard segments, the polymer becomes soft and moldable. Then, when strained, the SP molecules in the polymer matrix undergo isomerization, changing from the SP to MC structure. This transformation weakens its interaction forces with the polymer molecular chains, allowing the polymer soft segments to more freely rotate [24, 52, 53]. Some slight increases in $R_{\rm f}$ were observed with increased hard segment content, which was expected due to larger numbers of hydrogen bonding sites in these polymers. Hard segment content did not noticeably affect $R_{\rm r}$.

3.1.4 | Cytocompatibility

The live/dead assay performed on HDI5-PUR samples with the highest SP concentration showed high cytocompatibility with $99\%\pm0.2\%$ viability (Figure 3a). When cell viability was normalized to the original seeding density, all treatment groups showed viability above 100%; meaning there was cell proliferation during the experimental period, as shown in Figure S5. Therefore, the presence of PUR and PUR-SP did not hinder cell growth. Although more cell-material interaction studies on the PUR-SP are required before clinical use, this study provides initial safety proof of these materials for potential use as biosensing materials.

3.2 | Mechanochromic Behavior of PUR Films With SPs

3.2.1 | Influence of Polymer Hard Segment on Mechanochromism

All strained PUR-SP samples failed to show visible color changes in ambient light. However, the samples showed increased brightness and fluorescence under UV light and fluorescent microscopy and confocal microscopy (Figure 4a). Additionally, the 4HDI-SP and 6HDI-SP samples did not show visible color changes upon exposure to white light or UV light for 1h. In contrast, the 5HDI-SP samples exhibited a visible color change from yellow to pink (Figure 4b), when exposed to both UV and white light. This change is attributed to a shift in equilibrium between the SP (inactivated) and MC (activated) forms of the

TABLE 3 | Shape memory properties (shape fixity $[R_{\rm f}]$ and shape recovery $[R_{\rm r}]$) of PUR-SP samples measuring using dynamic mechanical analysis.

	4HDI		5HDI		6HDI	
SP content (%)	$R_{ m f}$	$R_{\rm r}$	$R_{ m f}$	$R_{\rm r}$	$R_{ m f}$	$R_{\rm r}$
0	0.77	0.96	0.79	0.94	0.83	0.95
0.015	0.75	0.95	0.75	0.90	0.77	0.93
0.032	0.74	0.94	0.75	0.95	0.82	0.94
0.063	0.74	0.94	0.73	0.94	0.82	0.94
0.126	0.76	0.96	0.80	0.93	0.81	0.94

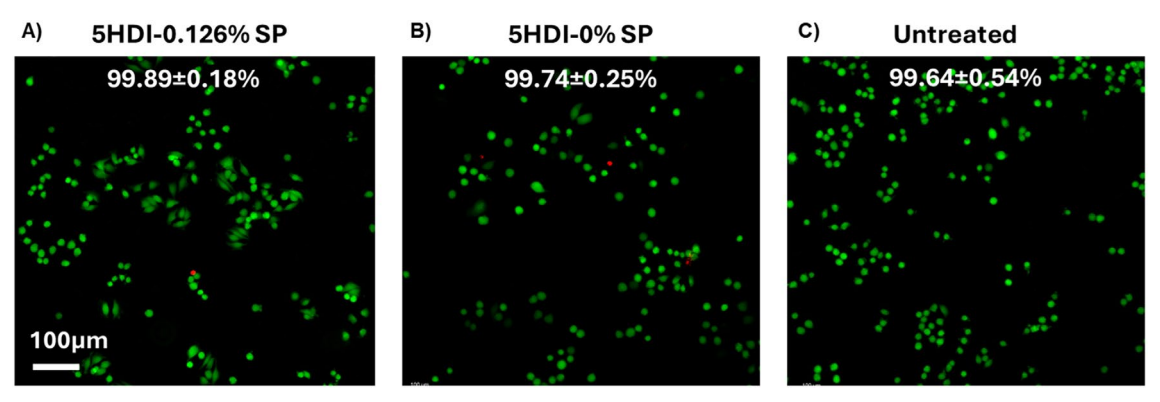


FIGURE 3 | Cytocompatibility assay (A) cells treated with 5HDI-0.0126% SP, (B) cells treated with pure PUR, and (C) untreated control cells. Mean \pm standard deviation displayed, n = 3.

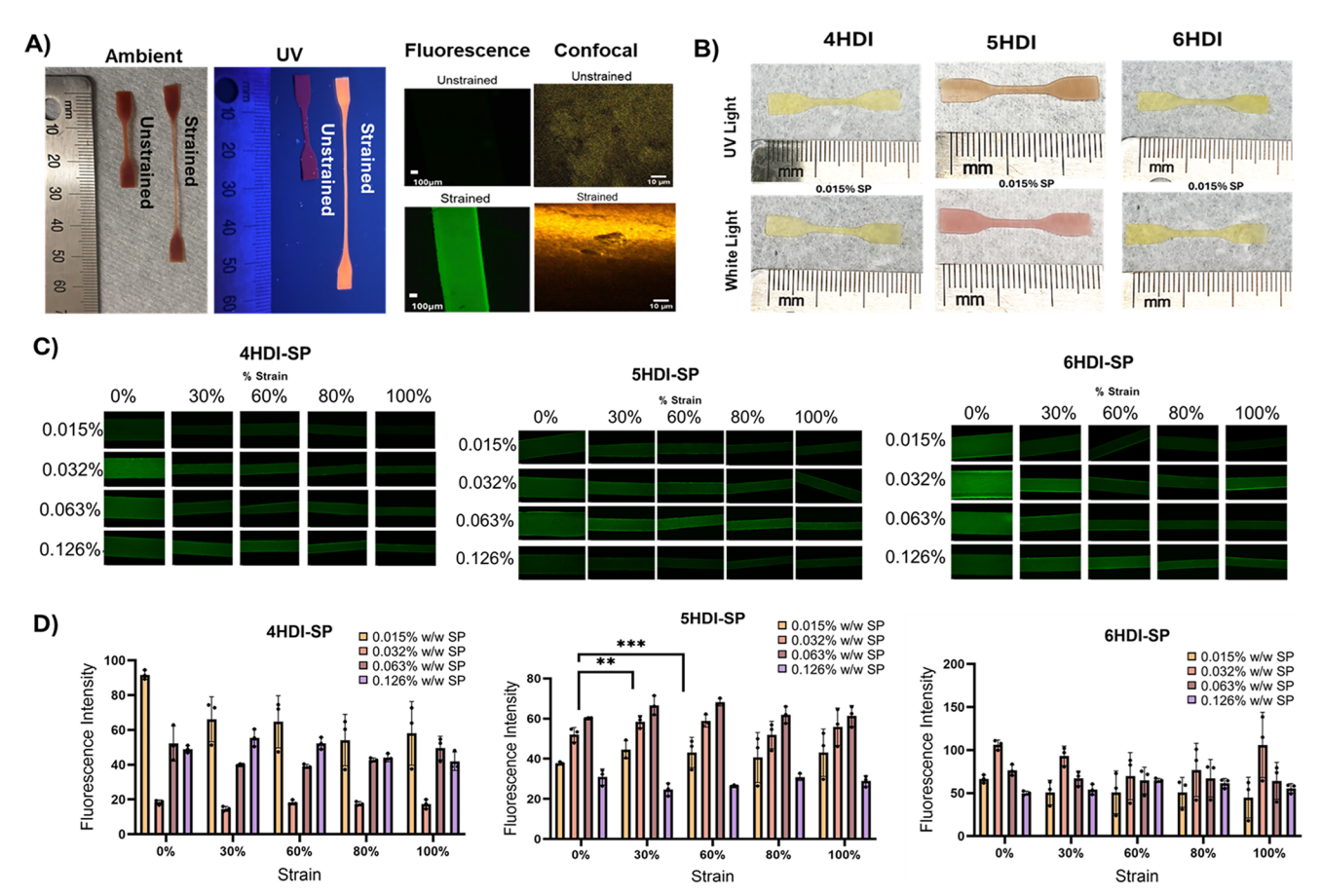


FIGURE 4 | Effects of strain on mechanochromic behavior. (A) Images of strained samples under ambient, UV, and fluorescent light. (B) Images of unstrained samples after exposure to UV light and white light. (C) Fluorescent images of strained PUR-SP samples. (D) Analysis of fluorescence intensity of PUR-SP samples at varying strains. Mean \pm standard deviation displayed, n = 3, ** $p \le 0.01$, and *** $p \le 0.001$ relative to control (sample with no strain).

mechanophore in the PUR, indicating that the unstrained 5HDI-SP provides sufficient spacing within the polymer matrix to enable the SP–MC transformation.

The mechanochromic behavior was further investigated by applying mechanical strain to the samples, followed by fluorescent imaging. The 4HDI-SP and 6HDI-SP samples did not show a linear pattern or clear trends in mechanochromism with increasing strain (Figure 4c,d). This observed mechanochromic behavior may be attributed to the solvatochromism

phenomenon. In that case, the solvent and/or the polymer matrix polarity could be responsible for a weak equilibrium between the SP and the MC forms. More polar solvents and polymer matrices have been known to displace the equilibrium toward the MC formation [40, 54–56]. Therefore, it is possible that 4HDI-SP samples and 6HDI-SP samples with lower and higher matrix polarity than 5HDI-SP samples resulted in no color changes even when the polymer sample was exposed to light or strained. Since the polymer hard to soft segment ratio affects the number of hydrogen bonds available in the polymer

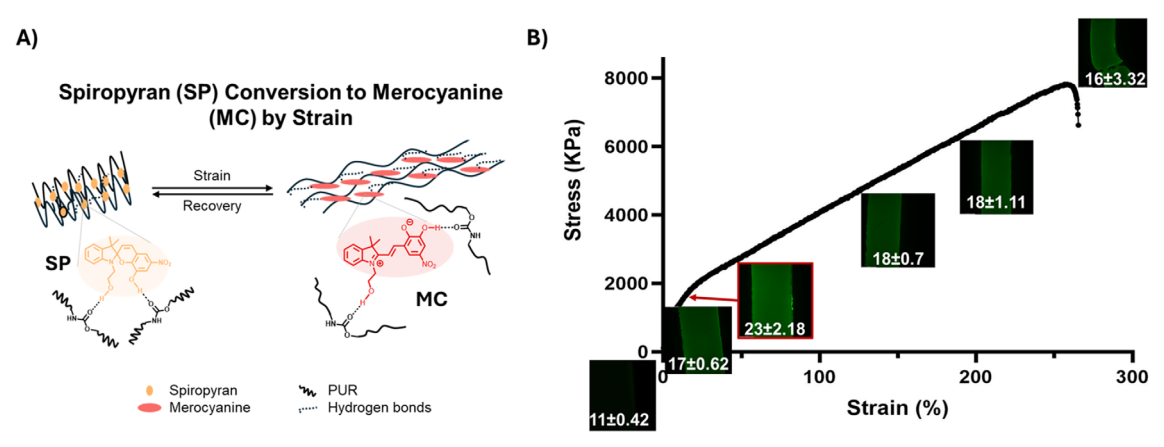


FIGURE 5 | Effect of engineering strain on mechanochromism. (A) Schematic representation of PUR straining process and its induction of SP to MC conversion. (B) Representative stress/strain curve of 5HDI-0.063% SP film with inset fluorescent images at each stage of tensile testing. Quantified fluorescence intensities are provided below each inset image and shown as mean \pm standard deviation; n = 3.

matrix, the ratio of H-bond interactions between the polymer backbone and incorporated SP could account for the variable trends in fluorescence observed in 4HDI-SP and 6HDI-SP samples [22, 24, 39, 41]. It is possible that only a portion of the SP was bonded to the polymer matrices, and a subset of incorporated SP could therefore not be activated by straining the polymer. In addition, the efficiency and pathways of mechanical force transduction across a polymer network are highly dependent on both the mechanical properties and structural characteristics of the polymer matrix [20]. The 4HDI-based system exhibits a lower crosslinking density and softer mechanical properties, which may lead to greater dissipation of mechanical energy within the network. As a result, the mechanical force may not be sufficiently transduced and applied to SP. In contrast, the 6HDI-based system is mechanically stiffer, which might prevent the network from achieving the optimal spacing required for efficient activation of densely packed SP units.

In contrast, Figure 4c,d shows that 5HDI-SP samples had consistent trends in terms of increased fluorescence intensity with increased SP concentration and/or strain. The 5HDI-SP samples with 0.063% SP had the highest fluorescence intensity (56% higher than unstrained samples, p < 0.05) in samples that were strained up to 130%. The 5HDI-SP samples with 0.126% SP had the lowest fluorescence intensity (32% lower than samples with 0.015% SP, p < 0.05), although they showed a similar trend in increasing fluorescence with strain. Fluorescence intensity has been found to be directly proportional to fluorophore concentration up to a certain point [20, 57-60]. When SP was mechanically activated, it acted as fluorophores and absorbed light. When the concentration of the fluorophore is high, the emitted light is absorbed by the fluorophore, causing a decrease in the observed fluorescence intensity. This is known as the "inner filter effect," a phenomenon that follows the Beer-Lambert Law [57, 61]. Therefore, at higher fluorophore concentrations, if fluorescence intensity is plotted against fluorophore concentration, it will begin increasing and then eventually deviate from linearity at higher concentrations. Since the 5HDI-PUR samples showed more promising and consistent trends in fluorescence change, these samples were chosen for further characterization of mechanochromic behavior.

3.2.2 | Influence of Engineering Stress on Mechanochromism

Dog bone-shaped samples were punched from the 5HDI-0.063% SP film and investigated under a strain rate of $10\,\mathrm{mm\,s^{-1}}$. In Figure 5b, stress is plotted as a function of strain. The curve is a typical stress–strain curve with a sigmoid shape exhibiting the elastic region, softening region, strain-hardening region, and failure. The Young's modulus, tensile strength, and elongation at break reached as high as $490\pm90\,\mathrm{kPa}$, $11,600\pm300\,\mathrm{kPa}$, and $370\%\pm45\%$, respectively.

The representative fluorescent images taken of the samples at each phase of deformation are shown alongside the stress–strain curve. As the films were stretched, their fluorescence started to increase. Stretching above the elastic region threshold (at the onset of deformation/plasticity) led to a sharp increase in fluorescence, indicating the ring-opening transformation from SP to MC. Figure 5a is a schematic representation of the process. As the specimen was further elongated, the fluorescence became slightly fainter. However, once the specimen failed, the intensity at the fracture appears higher than that of the overall sample. These findings are consistent with those reported by Cellini et al. [24], Zhang et al. [47], Davis et al. [62] who previously showed changes in color and fluorescence related to stress in mechanochromic polymer composites.

To estimate the threshold strain ratio, we performed ImageJ analysis of fluorescence intensity on representative images. As shown in Figure 5b, the fluorescence intensity was low at lower strain, then increased sharply at the onset of plastic deformation. We defined the threshold strain for SP activation as the point with the highest fluorescence intensity (red arrow), which under the 10 mm/s strain rate was estimated to be 2 MPa.

Initially, during elastic deformation, tensile strain was not transmitted to the SP molecule as it elongated and untangled the PUR chains [24]. When the strain reached approximately 25%, PUR chains began transmitting strain to the SP molecules, such that the SP structure was converted to MC, and the fluorescence increased. As the strain increased further, an increasing number

of SP structures were transformed into MC structures, resulting in a rapid increase in fluorescence.

Further experiments were conducted to determine the effect of strain rate on SP activation. Data in supplemental information (Figure S6) show that fluorescence increased with an increase in strain rate up to $10\,\mathrm{mm\,s^{-1}}$. However, when the strain rate was increased beyond $15\,\mathrm{mm\,s^{-1}}$, the fluorescence started to decline. This result indicates that the $10\,\mathrm{mm\,s^{-1}}$ strain rate is ideal for SP activation. These data correspond with previous work by Kim et al. [63], who found that SP activation was strain rate dependent. They showed that the fluorescence of their mechanochromic PMMA at a given strain was higher for slower strain rates, and at a given time was higher for faster strain rates.

3.2.3 | Effect of SP Concentration on Mechanochromism

UV-vis absorbance of 5HDI-SP films was investigated before and after straining to determine the influence of SP and strain on the absorption spectrum. An increase in the photochromic response was expected with increased SP concentration, where a higher conversion to MC was observed during straining. However, Figure 6a,b shows that the PUR/SP maximum absorbance did not vary linearly with the SP concentration. This nonlinearity between the maximum absorbance and SP concentration cannot be accounted for by the simple Beer–Lambert law [64]. However, it is important to note that the Beer–Lambert law is generally used to account for the absorbance of a solute in solution. This situation is quite different, as we measured the absorbance of a solute dissolved in a solid phase in this work.

Figure 6c shows that a maximum absorbance occurred at 410 and 550 nm. These peaks are associated with SP and MC, respectively [65, 66]. Further, the figure illustrates the influence of film thickness on absorbance. As expected from the Beer–Lambert law, the absorbance decreased with strain because of lower film thickness in the strained sample. Furthermore, it is noteworthy that even if samples were not strained, absorbance related to MC was detected, despite efforts to prevent any activation of the mechanophore prior to measurement. This absorbance behavior can be partially attributed to the phenomenon of solvatochromism mentioned earlier [56]. In that case, it is plausible that the polarity of the polymer matrix contributes to a minor degree of photochrome absorbance even before straining the sample [64, 67]. Further, when the area

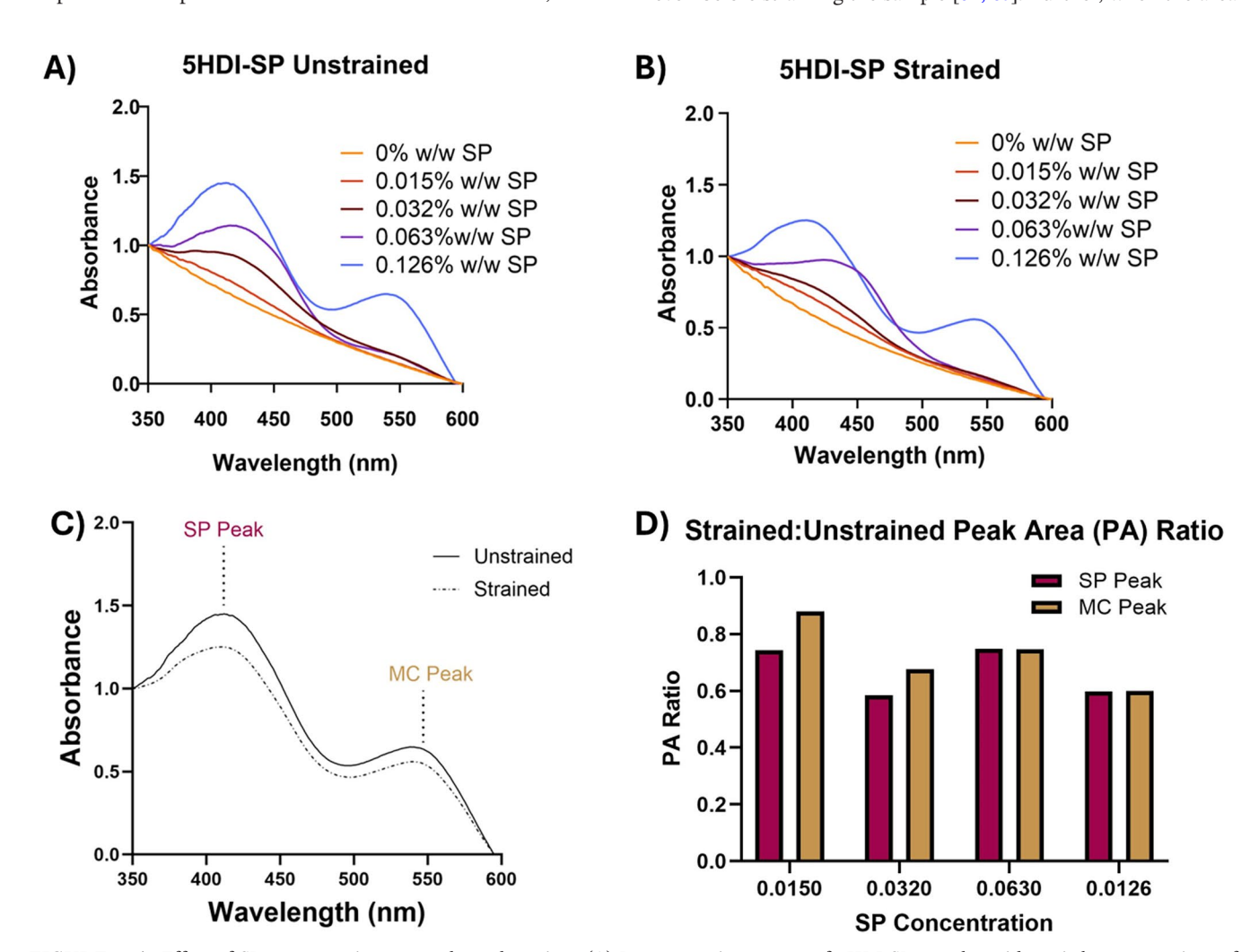


FIGURE 6 | Effect of SP concentration on mechanochromism. (A) Representative spectra of 5HDI-SP samples with varied concentrations of SP before strain. (B) Representative spectra of 5HDI-SP samples with varied concentrations of SP after strain. (C) Representative spectra of 5HDI-SP-0.126% SP before and after straining, where both the SP and MC peaks are visible. (D) Quantified peak area ratios for SP and MC in unstrained and strained samples.

under SP and MC peaks was quantified, the MC peak ratios were found to be larger in strained samples with lower concentrations of SP (up to 0.032%, Figure 6d). These findings indicate increased SP conversion to MC in strained samples, similarly to fluorescence data (Figure 4d) which showed increased fluorescence in strained 5HDI-SP samples with up to 0.063% SP, after which it plateaued.

3.2.4 | Influence of Shape Memory Process on Mechanochromism

5HDI-0.063% SP film samples with SP were then investigated to study how the shape memory process affects mechanochromism. Figure 7a shows DMA data with images taken (I) before heating, (II) after heating, (III) after straining and cooling, and (IV) after heating and recovery. As shown in the inset images of samples, strained PU/SP films displayed increased brightness when heated and strained, as expected based on other data. Here, we also observed reduced brightness after recovery, indicating that the shape recovery process can facilitate closure to MC to return to the SP isoform.

To confirm these results, the fluorescence of strained 5HDI-SP films was quantified during recovery on a heated confocal microscope stage (Figure 7b). This study showed an increase in fluorescence in the strained sample, which was reduced during recovery. Further validation was obtained using fluorescence microscopy imaging (Figure 7c). Samples that were strained and fixed in their temporary shape had increased fluorescence that was reduced after shape recovery via heating. These experiments

demonstrate the low fluorescence associated with the closed SP probe. After activation with force, the SP C—O bond is cleaved, and the photochromic probe becomes a metastable zwitterionic highly fluorescent MC [62, 64, 68]. Upon shape recovery and removal of forces holding chains apart that are applied during straining and fixation, this MC is converted back to the less fluorescent SP form.

The mechanochromic effect in PUR-SP provides a visual indication of the shape memory process by indicating strains applied and removed from the material during fixation and recovery. When the material is subjected to external force, such as tensile stress, the SP molecules within the PUR matrix undergo a structural change from the ring-closed SP to a ring-opened MC form. This change is accompanied by a brighter fluorescence transmission. This mechanochromic effect can therefore be useful in stress sensing to both monitor deformation and track the shape recovery processes. As the material returns to its original shape, the change in fluorescence can indicate the progress and completion of the shape recovery. Overall, the mechanochromic effect enhances the functionality of our shape memory PUR by adding a visual aspect to the mechanical properties, making them more versatile for applications in stress sensing systems.

3.3 | Effect of Bacterial Protease-Responsive Shape Recovery on Mechanochromism

As a proof of concept, we incorporated SP into our previously developed bacterial protease-responsive PUR (5HDI-PEP) [44].

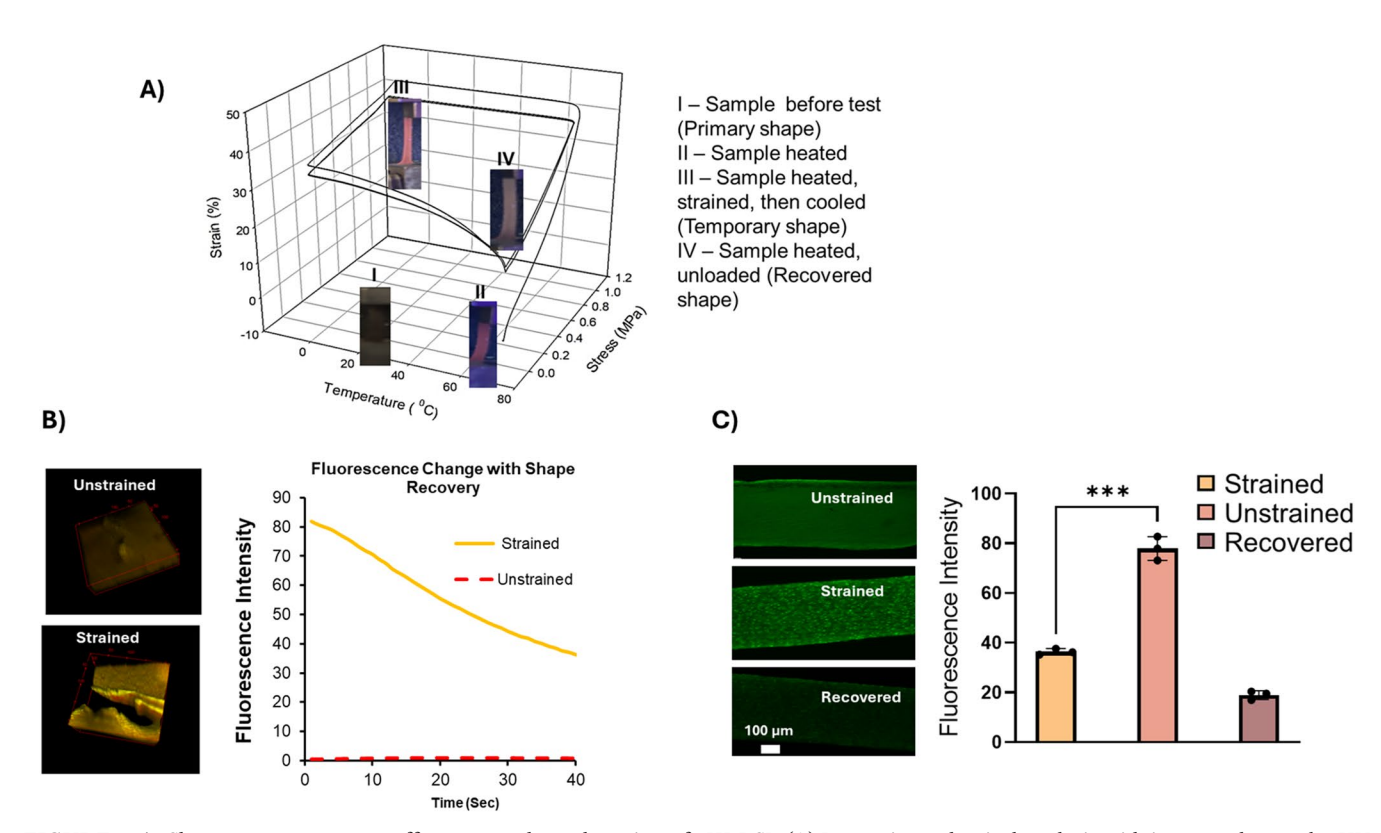


FIGURE 7 | Shape memory property effects on mechanochromism of 5HDI-SP. (A) Dynamic mechanical analysis with images taken under UV light during fixation and recovery. (B) Confocal microscopy images with quantified sample fluorescence during shape recovery induced by heating. (C) Fluorescence microscopy images and quantified fluorescence intensities after straining/fixing and after heating/recovering. Mean \pm standard deviation displayed, $n = 3 ***p \le 0.001$ relative to strained sample.

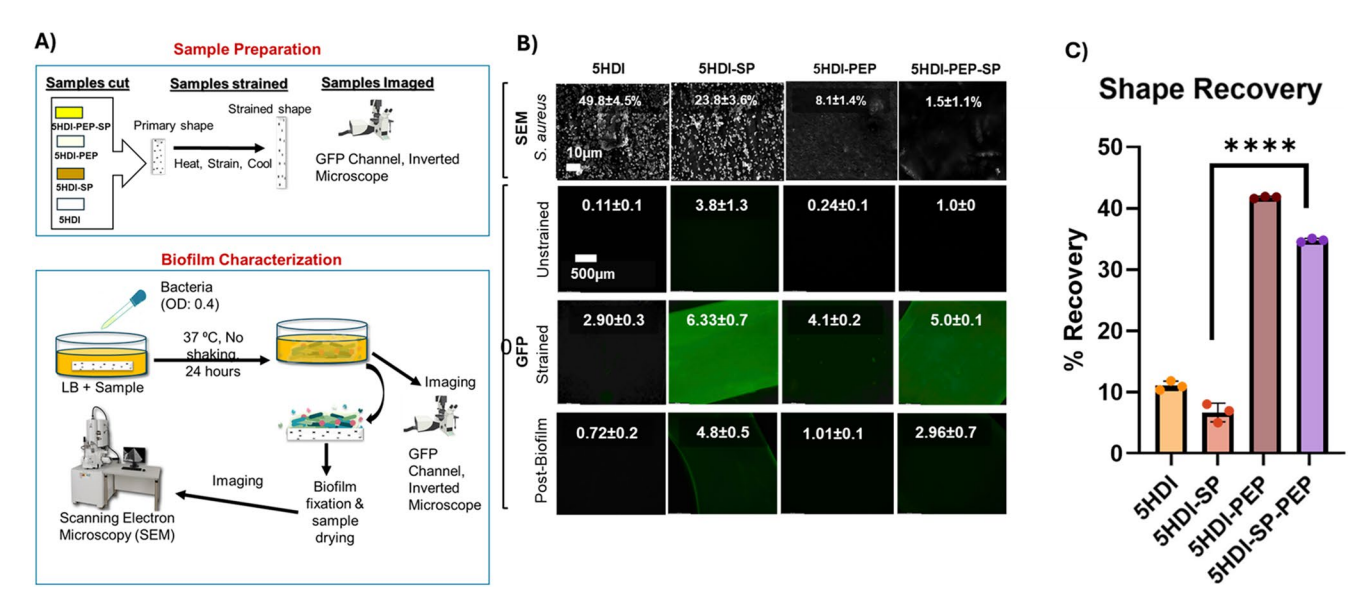


FIGURE 8 | Biofilm assay with SP-containing PURs. (A) Schematic representation of experimental process (B) SEM images of samples surfaces showing bacterial attachment and fluorescent images after 24h of exposure to *S. aureus*. Quantified percentage bacteria coverage and fluorescence intensity (green channel) is provided above each image and shown as mean \pm standard deviation, n = 3. (C) Percent shape recovery. Mean \pm standard deviation displayed, n = 3, ****p < 0.0001 relative to control (5HD-SP sample not protease responsive).

This SMP includes a small amount of peptide in its backbone (poly(glutamic acid)), which is cleaved by the V8 protease from S. aureus. Our prior work shows that these SMPs are highly stable in the presence of degradative agents and mammalian cells but undergo shape recovery in the presence of bacteria. This shape recovery is visible, and it prevents bacteria from forming biofilms on the PUR surface, providing a promising platform for future use in infection surveillance and prevention. After incorporating SP into the 5HDI-PEP, we prepared strained and non-strained (control) samples and performed a biofilm assay with S. aureus to determine whether bacteria-responsive shape recovery would result in mechanochromic effects. SEM images in Figure 8b show that biofilms form on control PUR surfaces with and without SP (5HDI and 5HDI-SP), which is similar to our previously reported results [44]. The strained bacteriaresponsive (5HDI-PEP and 5HDI-PEP-SP) samples underwent shape recovery after incubation with S. aureus for 24h, which resulted in biofilm disruption and minimal bacterial attachment to dressing material. Only isolated bacteria were observed on their surfaces. Thus, the inclusion of SP into the bacterial protease-responsive SMP does not negatively impact its biofilm inhibition capabilities.

To assess infection surveillance potential, fluorescent images were obtained of the samples before straining, after straining/ fixing, and after bacteria exposure, which induced shape recovery in the peptide-containing samples and did not affect the control sample dimensions (Figure 8c). Fluorescence intensity of 5HDI-SP increased after straining and reduced by ~24% after the biofilm assay, while the 5HDI-PEP-SP sample with increased fluorescence after straining exhibited an ~40% reduction in intensity after shape recovery during *S. aureus* exposure.

The release of SP from PUR-SP films under physiological conditions was investigated by incubating the films in PBS at 37°C.

The data in Figure S7 demonstrated that ~50%-60% SP is released from the strained PUR samples and ~25%-35% SP is released from the unstrained PUR samples over this time frame. The amount of SP released by strained and unstrained samples was not significantly different for both the 5HDI-SP and 5HDI-PEP-SP samples (p=0.78 and p=0.31 respectively). These findings demonstrate that the loaded SP molecules were relatively stable in the polymer matrix over a period of 8 days. This stability will help facilitate the application of the material as a sensor biomaterial for wound dressing, which would require a one-time use for up to 7 days.

This work demonstrates that mechanochromic biomaterials can be changed in a predictable way, providing an effective and convenient approach to the visualization and probing of specific biological interactions. Findings from this initial study convey the potential to apply PUR-PEP-SP in the surveillance of infections/biofilm by a color-changing mechanism. The use of fluorescence imaging to visualize changes in the material based on deformation or recovery of the shape is an obvious limitation. Future work will explore the use of other mechanophores in the PUR SMP to further characterize their potential for visible color-changing sensor applications.

4 | Conclusions

In this study, PUR-SPs with shape memory properties and mechanochromism were fabricated by adding small quantities of SP to a previously synthesized library of biostable segmented PURs with varying hard to soft segment ratios. All PUR-SPs showed high $T_{\rm g}$'s (> 80°C) and good shape memory performance, with shape fixation and shape $R_{\rm r}$ >73% and 90%, respectively. These properties are important as they enable maintenance of temporary shape upon exposure to

physiological conditions. Additionally, PUR-SPs showed excellent cytocompatibility (>99%). All PUR-SPs exhibited photochromic properties. However, only 5HDI-SP exhibited both photochromic and mechanochromic behaviors. It turned yellow-brown under 365 nm UV light irradiation and pink-red under white light. Tensile force resulted in increased fluorescence/brightness, which reduced or disappeared when the sample was recovered with heat. Successful fabrication and testing with *S. aureus* of 5HDI-PEP-SP demonstrated that the addition of stimuli-responsive components can enable specific responses, which can allow for biomedical application in instances such as in biofilm removal and infection surveillance in chronic wounds.

Acknowledgments

The authors would like to acknowledge seed funding from BioInspired Syracuse to support this work. Additionally, the authors would like to acknowledge Dr. Abrar Aljiboury from the Blatt Bioimaging Center at Syracuse University for assistance with confocal microscopy imaging and Dr. Xiaoran Hu, Chemistry Department, Syracuse University, for assistance with UV–Vis spectroscopy.

Conflicts of Interest

The authors declare no conflicts of interest.

Data Availability Statement

The data that support the findings of this study are available from the corresponding author upon reasonable request.

References

- 1. M. Ramezani and M. B. B. Monroe, "Biostable Segmented Thermoplastic Polyurethane Shape Memory Polymers for Smart Biomedical Applications," *ACS Applied Polymer Materials* 4 (2022): 1956–1965.
- 2. İ. N. Qader, M. Kök, F. Dagdelen, and Y. Aydoğdu, "A Review of Smart Materials: Researches and Applications," *El-Cezeri* 6 (2019): 755–788.
- 3. M. Mrinalini and S. Prasanthkumar, "Recent Advances on Stimuli-Responsive Smart Materials and Their Applications," *ChemPlusChem* 84 (2019): 1103–1121.
- 4. Z. L. Pianowski, "Recent Implementations of Molecular Photoswitches Into Smart Materials and Biological Systems," *Chemistry–A European Journal* 25 (2019): 5128–5144.
- 5. W. Yang, C. Liu, S. Lu, et al., "Smart On-Off Switching Luminescence Materials With Reversible Piezochromism and Basichromism," *ChemistrySelect* 2 (2017): 9215–9221.
- 6. C. T. Motz, V. Kabat, T. Saxena, R. V. Bellamkonda, and C. Zhu, "Neuromechanobiology: An Expanding Field Driven by the Force of Greater Focus," *Advanced Healthcare Materials* 10 (2021): 2100102.
- 7. W. E. King, G. Campbell, T. Gonis, et al., "Theory, Simulation, and Modeling of Interfaces in Materials—Bridging the Length-Scale Gap: A Workshop Report," *Materials Science and Engineering A* 191 (1995): 1–16.
- 8. B. S. Gomes, B. Simões, and P. M. Mendes, "The Increasing Dynamic, Functional Complexity of Bio-Interface Materials," *Nature Reviews Chemistry* 2 (2018): 1–15.
- 9. Y. Kim, E. C. Chica-Carrillo, and H. J. Lee, "Microfabricated Sensors for Non-Invasive, Real-Time Monitoring of Organoids," *Micro and Nano Systems Letters* 12 (2024): 26.

- 10. J. Sutlive, H. Xiu, Y. Chen, et al., "Generation, Transmission, and Regulation of Mechanical Forces in Embryonic Morphogenesis," *Small* 18 (2022): 2103466.
- 11. Y. Hwang and A. I. Barakat, "Dynamics of Mechanical Signal Transmission Through Prestressed Stress Fibers," *PLoS One* 7 (2012): e35343.
- 12. F. Alisafaei, X. Chen, T. Leahy, P. A. Janmey, and V. B. Shenoy, "Long-Range Mechanical Signaling in Biological Systems," *Soft Matter* 17 (2021): 241–253.
- 13. J. A. Sebastian, E. M. Strohm, J. Baranger, O. Villemain, M. C. Kolios, and C. A. Simmons, "Assessing Engineered Tissues and Biomaterials Using Ultrasound Imaging: In Vitro and In Vivo Applications," *Biomaterials* 296 (2023): 122054.
- 14. Y. Liu, L. Wang, L. Zhao, Y. Zhang, Z. T. Li, and F. Huang, "Multiple Hydrogen Bonding Driven Supramolecular Architectures and Their Biomedical Applications," *Chemical Society Reviews* 53 (2024): 1592–1623.
- 15. K. M. Hutchins, "Functional Materials Based on Molecules With Hydrogen-Bonding Ability: Applications to Drug Co-Crystals and Polymer Complexes," *Royal Society Open Science* 5 (2018): 180564.
- 16. M. Ramezani, D. Getya, I. Gitsov, and M. B. B. Monroe, "Solvent-Free Synthesis of Biostable Segmented Polyurethane Shape Memory Polymers for Biomedical Applications," *Journal of Materials Chemistry B* 12 (2024): 1217–1231.
- 17. J. Li, C. Nagamani, and J. S. Moore, "Polymer Mechanochemistry: From Destructive to Productive," *Accounts of Chemical Research* 48 (2015): 2181–2190.
- 18. Y. Chen, G. Mellot, D. van Luijk, C. Creton, and R. P. Sijbesma, "Mechanochemical Tools for Polymer Materials," *Chemical Society Reviews* 50 (2021): 4100–4140.
- 19. H.-A. Klok, A. Herrmann, and R. Göstl, "Force Ahead: Emerging Applications and Opportunities of Polymer Mechanochemistry," *ACS Polymers Au* 2 (2022): 208–212.
- 20. Q. Guo and X. Zhang, "A Review of Mechanochromic Polymers and Composites: From Material Design Strategy to Advanced Electronics Application," *Composites. Part B, Engineering* 227 (2021): 109434.
- 21. H. Traeger, Y. Sagara, J. A. Berrocal, S. Schrettl, and C. Weder, "Strain-Correlated Mechanochromism in Different Polyurethanes Featuring a Supramolecular Mechanophore," *Polymer Chemistry* 13 (2022): 2860–2869.
- 22. F. Zhang, R. Ji, N. Sun, et al., "Tunable Stress Transfer Efficiency of Polyurethane to Spiropyran by Multi-Functionalization and Its Effects on Mechano-Chromic Response," *Journal of Applied Polymer Science* 137 (2020): 49272.
- 23. L. Wang, L. Liu, B. Xu, and W. Tian, "Recent Advances in Mechanism of AIE Mechanochromic Materials," *Chemical Research in Chinese Universities* 37 (2021): 100–109.
- 24. D. A. Davis, A. Hamilton, J. Yang, et al., "Force-Induced Activation of Covalent Bonds in Mechanoresponsive Polymeric Materials," *Nature* 459 (2009): 68–72.
- 25. R. Klajn, "Spiropyran-Based Dynamic Materials," *Chemical Society Reviews* 43 (2014): 148–184.
- 26. H. Traeger, D. J. Kiebala, C. Weder, and S. Schrettl, "From Molecules to Polymers—Harnessing Inter- and Intramolecular Interactions to Create Mechanochromic Materials," *Macromolecular Rapid Communications* 42 (2021): 2000573.
- 27. W. Qiu, P. A. Gurr, and G. G. Qiao, "Color-Switchable Polar Polymeric Materials," *ACS Applied Materials & Interfaces* 11 (2019): 29268–29275.
- 28. A. Tork, F. Boudreault, M. Roberge, A. M. Ritcey, R. A. Lessard, and T. V. Galstian, "Photochromic Behavior of Spiropyran in Polymer Matrices," *Applied Optics* 40 (2001): 1180–1186.

- 29. F. M. Raymo and S. Giordani, "Signal Processing at the Molecular Level," *Journal of the American Chemical Society* 123 (2001): 4651-4652.
- 30. N. Ahmed, A. Kausar, and B. Muhammad, "Advances in Shape Memory Polyurethanes and Composites: A Review," *Polymer-Plastics Technology and Engineering* 54 (2015): 1410–1423.
- 31. P. Ping, W. Wang, X. Chen, and X. Jing, "The Influence of Hard-Segments on Two-Phase Structure and Shape Memory Properties of PCL-Based Segmented Polyurethanes," *Journal of Polymer Science, Part B, Polymer Physics* 45 (2007): 557–570.
- 32. F. Li, X. Zhang, J. Hou, et al., "Studies on Thermally Stimulated Shape Memory Effect of Segmented Polyurethanes," *Journal of Applied Polymer Science* 64 (1997): 1511–1516.
- 33. B. K. Kim, S. Y. Lee, and M. Xu, "Polyurethanes Having Shape Memory Effects," *Polymer* 37 (1996): 5781–5793.
- 34. Y. Huang, S. Huang, and Q. Li, "Mechanochromic Polymers Based on Mechanophores," *ChemPlusChem* 88 (2023): e202300213.
- 35. Y. Jiang, "An Outlook Review: Mechanochromic Materials and Their Potential for Biological and Healthcare Applications," *Materials Science and Engineering: C* 45 (2014): 682–689.
- 36. Y. Mao, Y. Kubota, R. Feng, et al., "Structure Reconfigurable Mechanochromic Polymer With Shape Memory and Strain-Monitored Function Enabled by a Covalent Adaptable Network," *Macromolecules* 55 (2022): 3948–3957.
- 37. N. Yenpech, V. Intasanta, K. Tashiro, and S. Chirachanchai, "Color and Shape Reversible, Recoverable and Repeatable Mechanochromic Shape Memory Polycaprolactone: A Single Material With Dual Functions," *Polymer Chemistry* 11 (2020): 91–101.
- 38. X. Wang, Y. He, and J. Leng, "Smart Shape Memory Polyurethane With Photochromism and Mechanochromism Properties," *Macromolecular Materials and Engineering* 307 (2022): 2100778.
- 39. X. Zhao, C. Whitney, J. Roman, A. Chattopadhyay, and L. L. Dai, "A Stress-Responsive Shape Memory Polymer via Chemical Grafting Functionalized Cinnamoyl-Based Mechanophore," in 38th Technical Conference of the American Society for Composites, ASC 2023. Proceedings of the American Society for Composites-Thirty-Eighth Technical Conference (ASC, 2023), 2131–2142.
- 40. W. Qiu, J. M. P. Scofield, P. A. Gurr, and G. G. Qiao, "Mechanochromophore-Linked Polymeric Materials With Visible Color Changes," *Macromolecular Rapid Communications* 43 (2022): 2100866.
- 41. M. Li, Q. Zhang, Y.-N. Zhou, and S. Zhu, "Let Spiropyran Help Polymers Feel Force!," *Progress in Polymer Science* 79 (2018): 26–39.
- 42. Z. Chi, X. Zhang, B. Xu, et al., "Recent Advances in Organic Mechanofluorochromic Materials," *Chemical Society Reviews* 41 (2012): 3878–3896.
- 43. Z. Wang, Z. Ma, Y. Wang, et al., "A Novel Mechanochromic and Photochromic Polymer Film: When Rhodamine Joins Polyurethane," *Advanced Materials* Deerfield Beach Fla 27 (2015): 6469–6474.
- 44. M. Ramezani and M. B. B. Monroe, "Bacterial Protease-Responsive Shape Memory Polymers for Infection Surveillance and Biofilm Inhibition in Chronic Wounds," *Journal of Biomedical Materials Research. Part A* 111 (2023): 921–937.
- 45. G. R. Gossweiler, G. B. Hewage, G. Soriano, et al., "Mechanochemical Activation of Covalent Bonds in Polymers With Full and Repeatable Macroscopic Shape Recovery," *ACS Macro Letters* 3 (2014): 216–219.
- 46. K.-P. Wang, Y. P. Deng, T. Wang, Q. D. Wang, C. G. Qian, and X. Y. Zhang, "Development of Spiropyran Bonded Bio-Based Waterborne Polyurethanes for Mechanical-Responsive Color-Variable Films," *Polymer* 210 (2020): 123017.

- 47. H. Zhang, Y. Chen, Y. Lin, et al., "Spiropyran as a Mechanochromic Probe in Dual Cross-Linked Elastomers," *Macromolecules* 47 (2014): 6783–6790.
- 48. R. Janissen and G. A. Filonenko, "Mechanochemistry of Spiropyran Under Internal Stresses of a Glassy Polymer," *Journal of the American Chemical Society* 144 (2022): 23198–23204.
- 49. X. Fang, H. Zhang, Y. Chen, Y. Lin, Y. Xu, and W. Weng, "Biomimetic Modular Polymer With Tough and Stress Sensing Properties," *Macromolecules* 46 (2013): 6566–6574.
- 50. C. Hudson, Studies of Segmented Polyurethanes for Blood Contacting Applications [Doctoral Dissertation McMaster University] (McMaster University Libraries Institional Repository, 1989).
- 51. T. J. Gately, W. Li, S. H. Mostafavi, and C. J. Bardeen, "Reversible Adhesion Switching Using Spiropyran Photoisomerization in a High Glass Transition Temperature Polymer," *Macromolecules* 54 (2021): 9319–9326.
- 52. C. K. Lee, D. A. Davis, S. R. White, J. S. Moore, N. R. Sottos, and P. V. Braun, "Force-Induced Redistribution of a Chemical Equilibrium," *Journal of the American Chemical Society* 132 (2010): 16107–16111.
- 53. C. K. Lee, B. A. Beiermann, M. N. Silberstein, et al., "Exploiting Force Sensitive Spiropyrans as Molecular Level Probes," *Macromolecules* 46 (2013): 3746–3752.
- 54. D. R. T. Roberts and S. J. Holder, "Mechanochromic Systems for the Detection of Stress, Strain and Deformation in Polymeric Materials," *Journal of Materials Chemistry* 21 (2011): 8256–8268.
- 55. A. Abdollahi, Y. Habibi, B. Ghasemi, and Z. Mohamadnia, "Solid-State Solvatochromism of Oxazolidine in Multi-Functionalized Copolymer Nanoparticles: Development of Advanced Materials With Multi-Color Fluorescence," *European Polymer Journal* 221 (2024): 113555.
- 56. A. Dey, A. Garai, V. Gude, and K. Biradha, "Thermochromic, Solvatochromic, and Piezochromic Cd(II) and Zn(II) Coordination Polymers: Detection of Small Molecules by Luminescence Switching From Blue to Green," *Crystal Growth & Design* 18 (2018): 6070–6077.
- 57. J. R. Lakowicz, ed., "Instrumentation for Fluorescence Spectroscopy," in *Principles of Fluorescence Spectroscopy* (Springer US, 2006), 27–61, https://doi.org/10.1007/978-0-387-46312-4_2.
- 58. D. Peak, T. C. Werner, R. M. Dennin, and J. K. Baird, "Fluorescence Quenching at High Quencher Concentrations," *Journal of Chemical Physics* 79 (1983): 3328–3335.
- 59. Y. Sagara, M. Karman, E. Verde-Sesto, et al., "Rotaxanes as Mechanochromic Fluorescent Force Transducers in Polymers," *Journal of the American Chemical Society* 140 (2018): 1584–1587.
- 60. W. Bae, T.-Y. Yoon, and C. Jeong, "Direct Evaluation of Self-Quenching Behavior of Fluorophores at High Concentrations Using an Evanescent Field," *PLoS One* 16 (2021): e0247326.
- 61. M. Tarai and A. K. Mishra, "Inner Filter Effect and the Onset of Concentration Dependent Red Shift of Synchronous Fluorescence Spectra," *Analytica Chimica Acta* 940 (2016): 113–119.
- 62. F. Cellini, L. Zhou, S. Khapli, S. D. Peterson, and M. Porfiri, "Large Deformations and Fluorescence Response of Mechanochromic Polyurethane Sensors," *Mechanics of Materials* 93 (2016): 145–162.
- 63. J. W. Kim, Y. Jung, G. W. Coates, and M. N. Silberstein, "Mechanoactivation of Spiropyran Covalently Linked PMMA: Effect of Temperature, Strain Rate, and Deformation Mode," *Macromolecules* 48 (2015): 1335–1342.
- 64. A. D. Pugachev, E. L. Mukhanov, I. V. Ozhogin, A. S. Kozlenko, A. V. Metelitsa, and B. S. Lukyanov, "Isomerization and Changes of the Properties of Spiropyrans by Mechanical Stress: Advances and Outlook," *Chemistry of Heterocyclic Compounds* 57 (2021): 122–130.
- 65. Y. Kalisky, T. E. Orlowski, and D. J. Williams, "Dynamics of the Spiropyran-Merocyanine Conversion in Solution," *Journal of Physical Chemistry* 87 (1983): 5333–5338.

- 66. A. K. Chibisov and H. Görner, "Photoprocesses in Spiropyran-Derived Merocyanines," *Journal of Physical Chemistry. A* 101 (1997): 4305–4312.
- 67. F. Ciardelli, G. Ruggeri, and A. Pucci, "Dye-Containing Polymers: Methods for Preparation of Mechanochromic Materials," *Chemical Society Reviews* 42 (2013): 857–870.
- 68. M. Mandal, D. Banik, A. Karak, S. K. Manna, and A. K. Mahapatra, "Spiropyran–Merocyanine Based Photochromic Fluorescent Probes: Design, Synthesis, and Applications," *ACS Omega* 7 (2022): 36988–37007.

Supporting Information

Additional supporting information can be found online in the Supporting Information section. **Data S1:** Supporting information.